Supplementary Information for *Optical detection of a single rare-earth ion in a crystal*

R. Kolesov[1], K. Xia[1], R. Reuter[1], R. Stöhr[1], A. Zappe[1], J. Meijer[2], P.R. Hemmer[3], and J. Wrachtrup[1]

[1] 3. Physikalisches Institut, Universität Stuttgart and Stuttgart Research Center of Photonic Engineering (SCoPE), Pfaffenwaldring 57, Stuttgart, D-70569, Germany
[2] Ruhr-Universität Bochum, RUBION, Bochum, D-44780, Germany
[3] Department of Electrical & Computer Engineering, Texas A&M University, College Station, TX 77843-3128, USA

Supplementary Figures

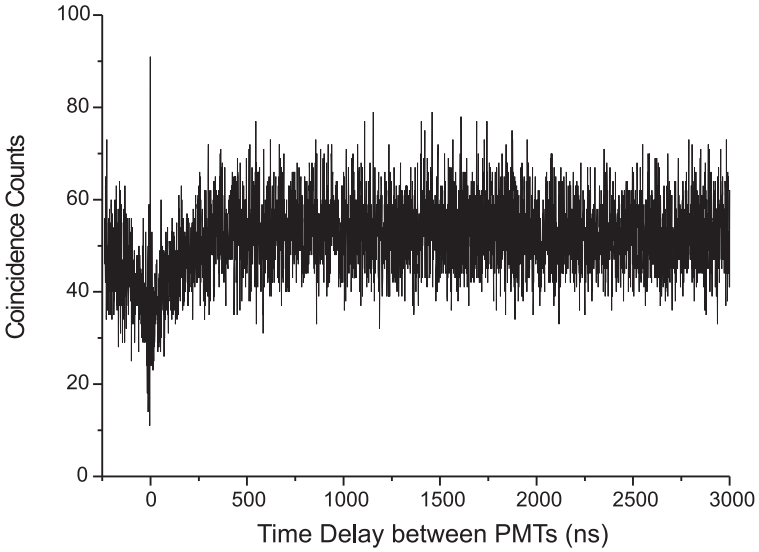

Supplementary Figure S1: **Anti-bunching signal from a single Pr^{3+} in a bulk YAG crystal.** Photon antibunching signal from a single Pr^{3+} ion in a high purity YAG crystal obtained from Scientific Materials Corp. With the estimated density of 0.6 $ions/\mu m^3$ the residual background from the praseodymium ions out of laser focus accounts for 35% of the collected fluorescence. This explains shallow antibunching dip at zero time delay.

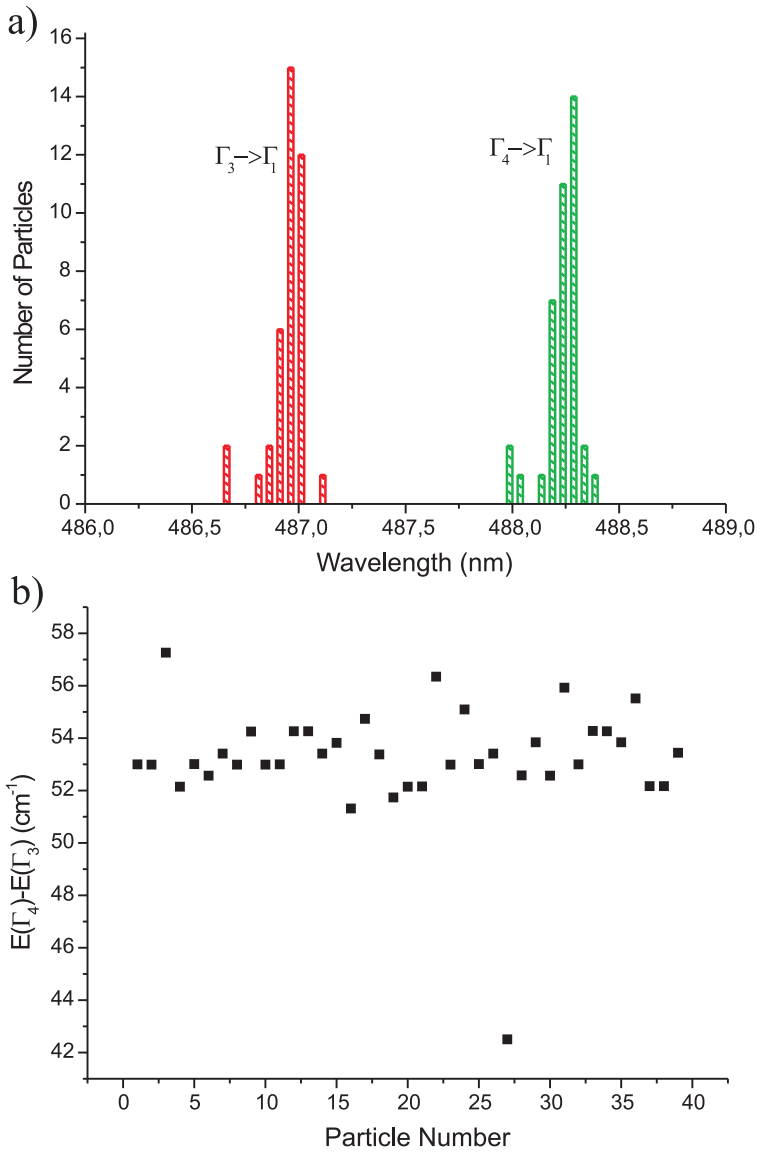

Supplementary Figure S2: **Statistical distribution of excitation lines.** a) Statistical distribution of the positions of two excitation lines in the vicinity of $^3H_4 \rightarrow ^3 P_0$ excitation transition. 39 single Pr^{3+} centers are evaluated. b) Statistical distribution of the splitting between Γ_3 and Γ_4 sublevels of $^3H_4$ state. The average value of 53.5 cm^{-1} is in good agreement with the splitting of ≈ 50 cm^{-1} known from the bulk measurements.

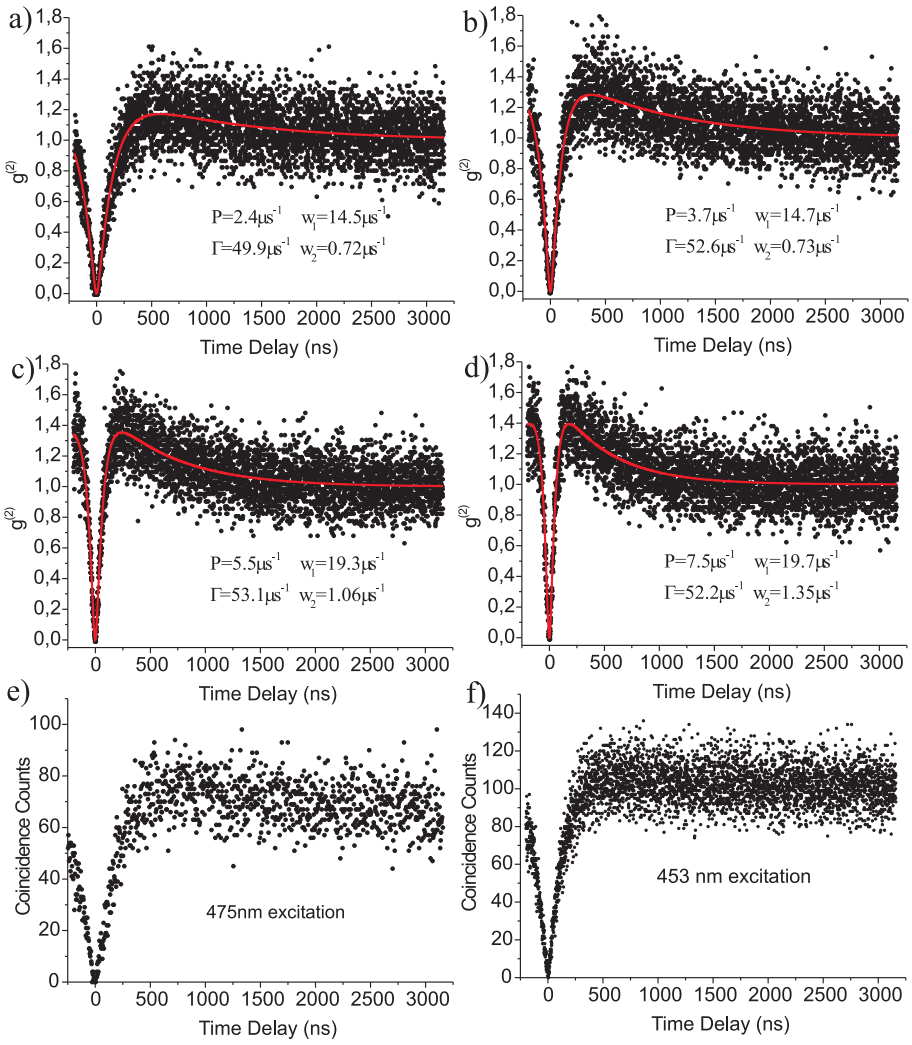

Supplementary Figure S3: **Anti-bunching signals at different excitation conditions.** a), b), c), and d) show antibunching signals obtained with excitation powers of 1.5 mW, 2.5 mW, 3.5 mW, and 4.5 mW at 488.2 nm, respectively. The deduced parameters of pumping, radiative decay, and metastable state population/depopulation rates are indicated. e) and f) show antibuncing curves taken on spot 1 (see main text) with 475 nm and 453 nm excitation, respectively.

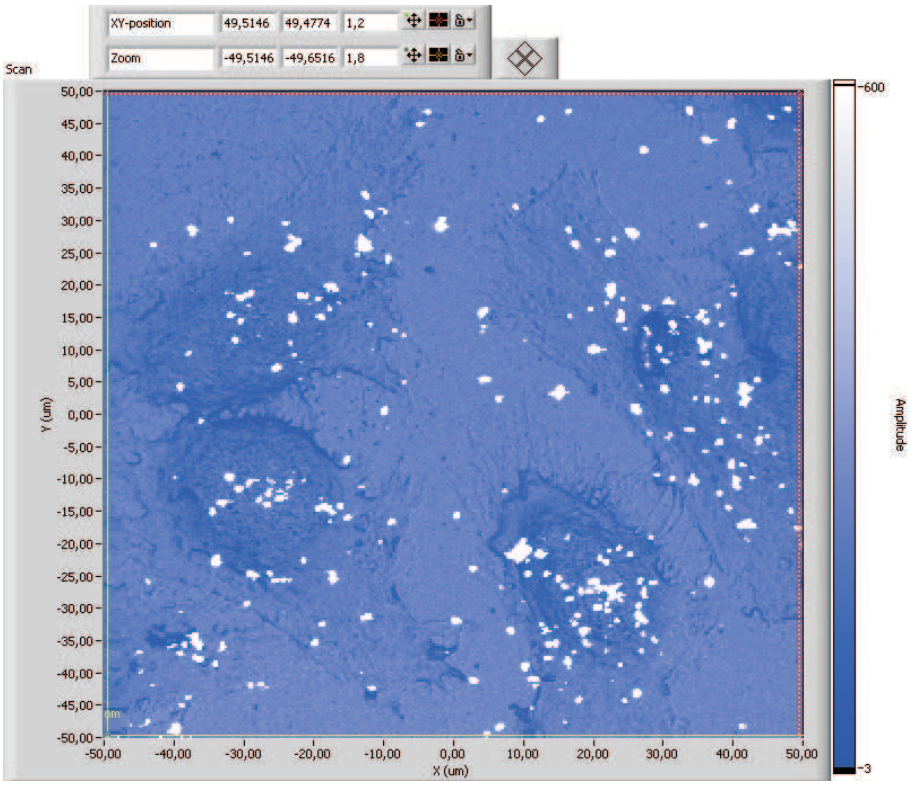

Supplementary Figure S4: $Pr^{3+} : YAG$ **nanoparticles in HeLa cells.** Upconversion fluorescence image of $Pr : YAG$ nanoparticles and nanoparticle clusters inside fixed HeLa cells. Prior to the experiment the cell culture was incubated with an addition of colloidal suspension of $Pr : YAG$ nanoparticles and, subsequently, fixed. The white spots on the scan indicate the position of the nanoparticles and their clusters. For fluorescence detection low OD 450 nm shortpass filter was used in order to visualize cell boundaries by scattered excitation laser light (473 nm). Otherwise, as a consequence of background-free nature of upconversion imaging of $Pr : YAG$ nanocrystals, only the nanoparticles are visible, but not the cells.

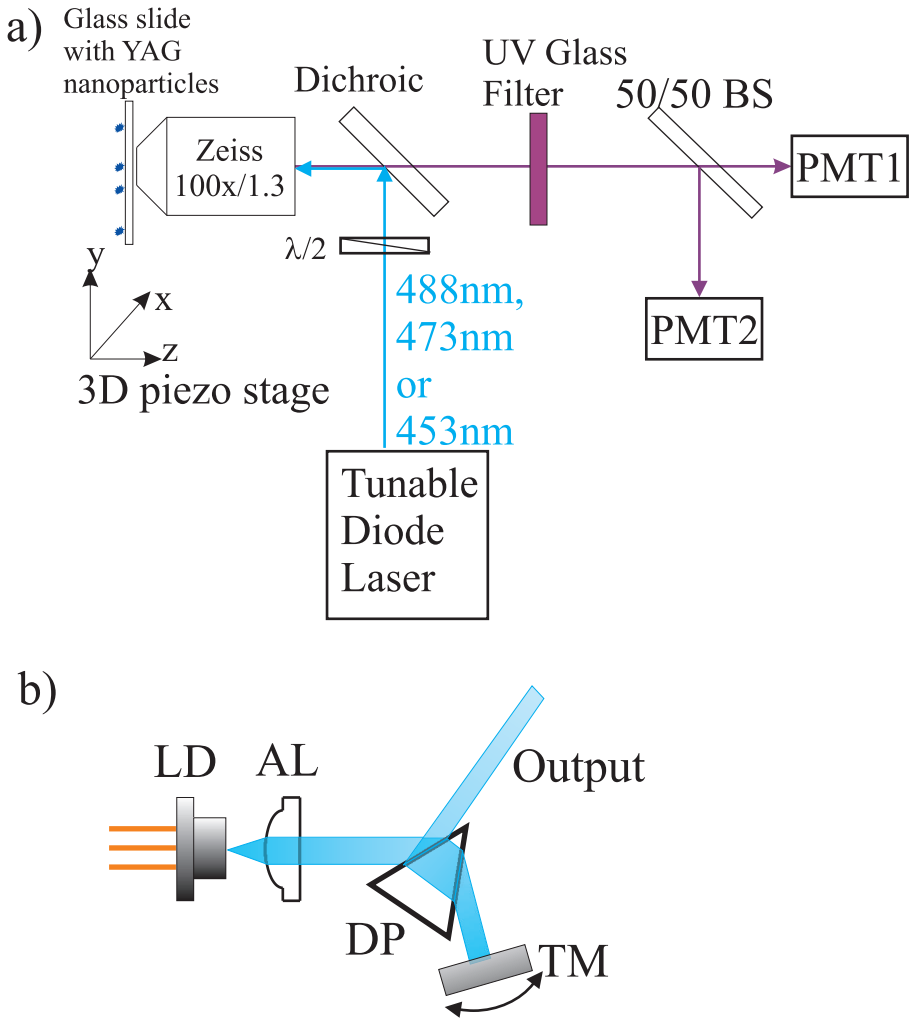

Supplementary Figure S5: **Layout of a UV upconversion microscope.** a) Experimental setup used for studying single emitting Pr^{3+} centers in YAG nanoparticles. b) Laser diode tuning in the external cavity. Abbreviations stand for: LD - laser diode, AL - aspheric lens, DP - dispersion prism, and TM - tuning mirror. See Methods section for details.

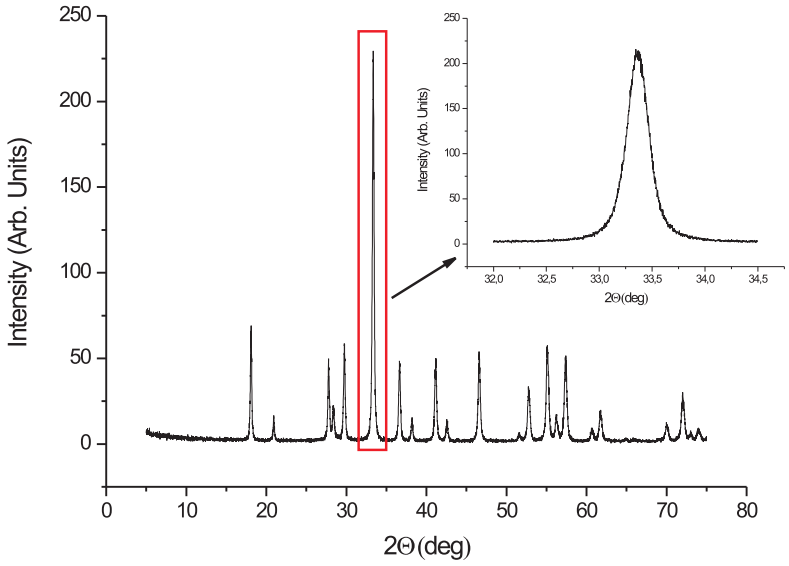

Supplementary Figure S6: **XRD spectrum of $Pr^{3+} : YAG$ nanoparticles.** The size of single crystalline core estimate of 32 nm is based on the width of the main peak (zoomed on the inset).

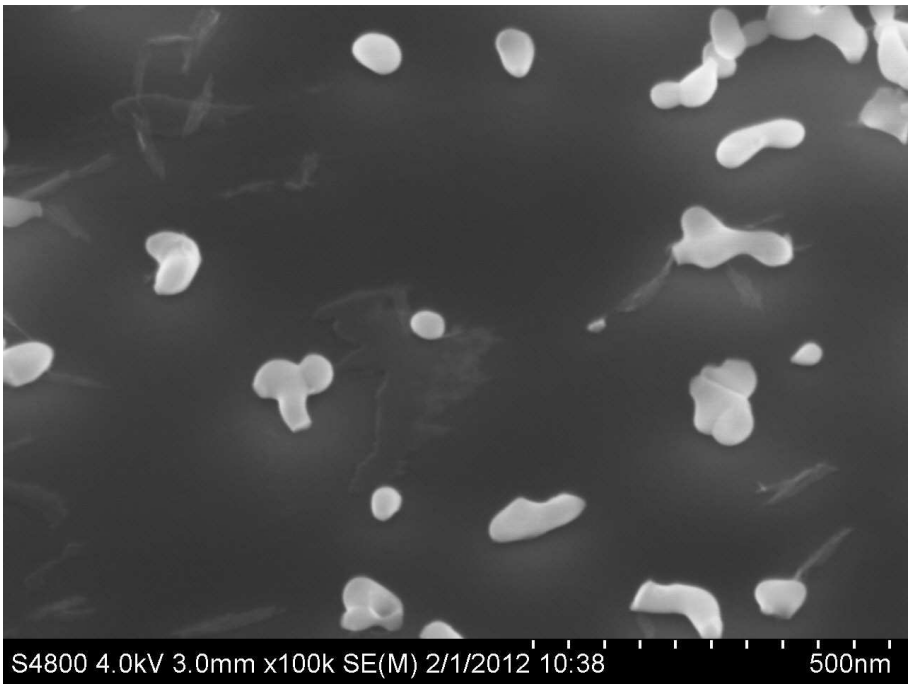

Supplementary Figure S7: **SEM scan of $Pr^{3+} : YAG$ nanoparticles.** The particles were dried on the silicon substrate out of isopropanol suspension. Upon drying, most particles cluster though a few individual nanocrystals can be seen.

Supplementary Tables

Particle number	Original fluorescence (kcounts/sec)	Fluorescence after development (kcounts/sec)	Enhancement factor
1	98.8	573	5.8
2	12.2	94.6	7.8
3	31.1	171	5.5
4	16.7	138	8.3
5	62.8	318	5.1
6	45.7	361	7.9
7	53.6	455	8.5
8	75.3	562	7.5
9	113	553	4.9
10	6.9	45.8	6.6
11 (ref)	44.4	43.1	0.97
12 (ref)	74.9	70.5	0.94

Supplementary Table S1: **Fluorescence detection enhancement due to self-assembled SILs.**

Supplementary Methods

Analysis of the setup collection efficiency

Our analysis of UV transmission of optical elements constituing our microscope (i.e. objective lens, dichroic mirror, and UG11 filter) shows that at most 25% of the photons emitted within the collection solid angle of the objective lens can reach the detector, whose efficiency is 30%. The numerical aperture of the objective lens being used is 1.30 meaning that the collection solid angle is close to π. Thus, 25% of the photons emitted by Pr^{3+} ion start propagating towards the detectors. All together, only 1.8% of the emitted photons produce a click on the detectors. At the same time, the decay parameters deduced from antibunching curve in Supplementary Fig.S3d yield the population of the emitting $4f5d(1)$ state to be 2.3% with 33% being in the metastable state at the excitation power of 4.5 mW (488.2 nm). This gives us an emission rate of 1.18×10^6 $photons/s$ and, correspondingly, ≈ 21 $kcounts/s$ of the detected count rate, in farely good agreement with the experimentally measured 14 $kcounts/s$. The above analysis shows that Pr^{3+} center is much brighter than seen by our microscope and that optimization of collection efficiency is required.

Creation of a solid immersion lens for $Pr^{3+} : YAG$ nanoparticle

UV emission of a $Pr : YAG$ nanoparticle under visible excitation can induce photochemical reaction in the surrounding of the nanoparticle. For instance, it can initiate cross-linking of a negative tone photoresist. If the nanoparticle is lying on a glass surface and covered by a photoresist layer, its UV emission can induce cross-linking in the nearest hemisphere (Fig.5a of the main text) whose radius depends on the exposure duration and brightness of the UV emission. After development, the cross-linked hemisphere would present a solid immersion lens for the nanoparticle whose emission created the hemisphere.

In the present case, SIL production was accomplished in the following way. $Pr : YAG$ nanoparticles (0.3% praseodymium concentration) were spin-coated on a marked glass slide. At first, a map of nanoparticles in a certain area of the sample was created. At that time, an objective lens without immersion (Melles Griot, 0.85NA) and 488.2 nm excitation laser were used. The excitation power was set to 100 μW and the fluorescent yields of 12 nanoparticles within the scan area of 100×100 μm^2 were recorded. After that, the sample was covered with thick ($10 - 20$ μm) layer of negative tone photoresist (SU-8). After prebaking for 10 minutes at $95°C$, the sample was transferred back to the microscope. Due to the markers present on the glass surface, it was possible to find the sample area mapped at the first step. This time, oil immersion objective lens (Zeiss Fluar UV, 100x1.3NA) was used to illuminate the particles. The power of the excitation beam (488.2 nm) was reduced to 10 μW to scan through the sample and find the positions of the 12 nanoparticles identified at the first step. After that, 10 of the 12 nanoparticles were exposed by 100 μW of 488.2 nm laser

for about 2 minutes each. After exposure, the sample was baked at $95°C$ for 3 minutes and subsequently developed in PGMEA. As a result, 10 SILs with radii between 2 and 5 microns depending on the brightness of the corresponding particle were created. The typical shape of such a SIL is shown in Fig.5b of the main text. Finally, the estimate of fluorescence collection enhancement was done by the immersionless objective lens having 2 unexposed nanoparticles as references. The emission yield of the later remained the same under 100 μW excitation while the fluorescent yield of the exposed nanoparticles increased 5-8.5 times as indicated in the Supplementary Table S1. The last 2 nanoparticles were not exposed and showed no fluorescence enhancement.